Electronic structure and lattice instability of metallic VO_2†

Michèle Gupta* and A. J. Freeman
Physics Department and Materials Research Center, Northwestern University, Evanston, Illinois 60201 and Argonne National Laboratory, Argonne, Illinois 60439

D. E. Ellis
Physics Department and Chemistry Department, Northwestern University, Evanston, Illinois 60201
(Received 6 June 1977)

A first-principles energy-band study of the metallic rutile phase of VO_2 using a general crystal potential and an expansion of the Bloch functions in a linear combination of atomic orbitals is reported. The results are compared with previous work and experimental optical, x-ray absorption and emission, and x-ray photoelectron spectroscopy data. We obtain a large density of states at the Fermi energy; the Fermi surface is found to be determined by the two lowest d bands, at the bottom of the "t_{2g}" manifold which is split by the orthorhombic field; the lowest-band Fermi surface possesses some nesting features corresponding to a nesting vector $\vec{q} = \Gamma R$. A calculation of the generalized susceptibility in the constant-matrix-element approximation shows the existence of a maximum at the zone boundary R. We suggest that the formation of a charge-density wave with wave vector $\vec{q} = \Gamma R$ accompanied by a periodic lattice distortion is thus possible; the subsequent condensation of phonons at the point R could then explain the crystallographic phase transition observed at $T = 339$ K.

I. INTRODUCTION

Vanadium dioxide undergoes a crystallographic phase transformation at $T_c = 339 \pm 1$ K from the monoclinic distorted rutile structure to the tetragonal rutile structure which is accompanied by an abrupt jump in the metallic conductivity[1,2] [from 10^{-2} to 10^4 $(\Omega\ \mathrm{cm})^{-1}$] and a jump in the magnetic susceptibility[3] [from 6.5×10^{-5} to 6.7×10^{-4} emu/mole]. This semiconductor to metallic phase transformation has been studied very extensively both experimentally and theoretically.[4] Unlike V_2O_3 and other transition-metal compounds known as "Mott-Hubbard insulators" which show antiferromagnetic ordering in the low-temperature phase, VO_2 remains paramagnetic below T_c and no long-range magnetic order is observed either in magnetic susceptibility,[5] Mössbauer,[6] or nuclear-magnetic-resonance experiments.[7] The semiconducting monoclinic phase of VO_2 is characterized by a pairing of the vanadium atoms along the c axis resulting in a doubling of the unit-cell size; along the c axis one finds alternatively short and long metal-metal distances[8,9]; at the same time, each vanadium "pair" is tilted with respect to the c axis, the vanadium atoms being no longer at the center of the distorted ligand octahedron. It is also worth noting the large further distortion of the octahedral geometry in the low-temperature phase, with an important shortening of some of the V-O bonds.[9] This pairing of the vanadium atoms can explain the lack of localized moments and account for the magnetic properties and possibly some of the electrical properties of the semiconducting phase, as the electrons may now be trapped in homopolar bonds.[10] This picture has been also useful in accounting for some features of the magnetic behavior[11] of the alloy $V_{1-x}Nb_xO_2$ with $x \leq 0.5$.

A. Electronic-structure models

These structural peculiarities led Goodenough[10] to propose a model of the electronic structure which can explain some properties of the metallic and semiconducting phases. This model is based on molecular orbital theory in conjunction with crystal field and chemical bonding ideas. In the metallic state, the interaction of cations along the c axis gives rise to a narrow $d_{\parallel}$ band which is overlapped by a wider π^* band formed by antibonding vanadium d and oxygen p_π states. In the low-temperature phase, the crystal distortion is thought to be responsible for three effects: (i) the π^* band rises above the Fermi level due to a stronger vanadium d-oxygen p_π interaction, resulting from the shortening of the distance of the vanadium to one oxygen atom; (ii) the $d_{\parallel}$ band splits due to the pairing of V atoms along the c axis; (iii) the lowest part of the $d_{\parallel}$ band is filled and separated by a small gap from the upper part, thereby accounting for the semiconducting properties of the compound.

The essential features of the electronic structure of the metallic phase of VO_2 proposed by Goodenough[10] have been confirmed by the band-structure calculation of Caruthers *et al.*,[12] using the combined augmented-plane-wave–linear-combination-of-atomic-orbitals (APW-LCAO) inter-

polation scheme. Studies in the tight-binding formalism have been outlined by Mitra *et al.*[13]; the same authors[14] also obtained limited APW band results for metallic VO_2. More recently, several rutile structure oxides have been studied by Mattheiss[15] using the combined APW-LCAO method, while Daude *et al.*,[16] applied the tight-binding and pseudopotential method to the study of the electronic structure of TiO_2.

The validity of a band-structure description of the high-temperature phase of VO_2 is quite widely admitted; optical[17] and x-ray photoelectron measurements[18,19] have revealed that the *d*-band width in the vanadium oxides is not too narrow and so correlation effects in the metallic phase might be less important than was originally thought. Thus, the experimental data concerning the metallic phase appear to indeed be compatible with a band model, as noted recently by Zylbersztein and Mott.[20]

In the semiconducting phase, electronic correlation effects play an important role,[20,21] and the validity of a band-structure description is questionable. We should note, however, that Caruthers *et al.*,[22] starting from tight-binding parameters determined for the band structure of the metallic phase, were able to find a new set of parameters which could account for the experimental semiconducting gap in the low-temperature phase.

B. Driving mechanism of the structural transformation

Several models have been proposed to explain the phase transition of VO_2. The phenomenological model of Goodenough[10] of a metal to semiconductor phase transition driven by a lattice distortion was made more quantitative by Adler and Brooks,[23] and Adler *et al.*[24] The role of the crystalline distortion was also emphasized by Berglund and Guggenheim,[25] Paul,[26] and Hearn.[27] On the other hand, experimental evidence, such as the large magnetic susceptibility of metallic VO_2 which decreases as T increases, has drawn the attention of the theorists to the importance of electronic correlation effects. Brinkman and Rice[21] interpreted the magnetic susceptibility of metallic VO_2 by invoking spin fluctuations in a highly correlated electron gas. The importance of the electronic correlation effects in the insulating phase has also been invoked to interpret the magnetic and electric properties[28,29] of alloy systems such as $V_{1-x}Cr_xO_2$ and $V_{1-x}Nb_xO_2$.

Aside from the possible role of electronic correlations, the role of the lattice in the phase transition (through the electron-phonon coupling) is demonstrated by several experimental facts. The large entropy of the transition $\Delta S \simeq 3$ cal/(mole K) cannot be accounted for by an electronic contribution, which was estimated to be only ~0.3 cal/(mole K) by Ladd[30] and ~1 cal/(mole K) by Zylbersztejn and Mott.[20] Paul[26] first suggested that the major change in the entropy (and hence the reduced free energy of the metallic phase) is due to soft-phonon modes. Although inelastic-neutron-scattering experiments are not available for VO_2, due to the large incoherent-scattering cross section of vanadium, the study of the Raman spectrum of metallic and semiconducting VO_2 by Srivastava and Chase[31] showed a pronounced softening in the phonon spectrum for the metallic phase. The large broadening of the phonon structure from the semiconducting to the metallic phase of VO_2 (contrary to what is observed[32] for V_2O_3) is evidence for a large electron-phonon coupling in the high-temperature phase. The structural disorder of the metallic phase manifests itself by an anomalously large dilation coefficient along the *c* axis which indicates strong anharmonic effects; the anharmonic interactions could then lead to a temperature renormalization of some phonon frequencies. It is also worth noting in this connection that the V-V distance along the *c* axis is shorter in VO_2 than in the rutile phases of TiO_2 or CrO_2. The lattice softening of the rutile phase is also suggested by a lower value of the Debye temperature Θ_D in the metal.[33] This x-ray diffraction study showed a large Debye-Waller factor in metallic VO_2, and was ascribed to a value of Θ_D 105° lower than in the other phase.[33] A similar observation was made[34] also for $V_{0.976}Cr_{0.024}O_2$. The large thermal displacements found for the metallic phase are compatible with a possible soft-mode-driven phase transformation.

Similar compounds like NbO_2 or the alloys $V_{1-x}Nb_xO_2$ show some indication of a possible soft-phonon-driven lattice instability: NbO_2 is isoelectronic to VO_2 and undergoes (at a higher temperature $T_c = 1081 \pm 2$ K) a crystallographic phase transformation from the body-centered-tetragonal to the rutile structure accompanied by a semiconducting to metallic phase transition. A neutron-scattering study of the phase transformation of NbO_2 by Shapiro *et al.*,[35] revealed the existence of critical scattering above T_c; the phase transformation was then interpreted as being driven by a soft-mode instability of wave vector $\vec{q} = (\frac{1}{4}, \frac{1}{4}, \frac{1}{2})$ in the rutile phase. The $V_{1-x}Nb_xO_2$ systems have also been extensively studied; Comès *et al.*[36] observed strong diffuse x-ray scattering from $V_{0.9}Nb_{0.1}O_2$ along a rod in reciprocal space with wave vector $\vec{q} = (\xi, \frac{1}{2} - \xi, \frac{1}{2})$, $0 \leq \xi \leq \frac{1}{2}$ joining the points R of the Brillouin zone of the tetragonal phase. For VO_2, a group-theory analysis[37] shows that the phase transformation is com-

patible with (but not unique to) a soft phonon at the point R, $\vec{q} = (\frac{1}{2}, 0, \frac{1}{2})$ in the rutile structure being "frozen in" at the transition. A recent study[38] of the temperature variation of the ultrasonic attenuation and phase velocity in VO_2 provides further evidence for the existence of a soft mode at R.

In this paper, we investigate whether the electronic properties, e.g., Fermi-surface geometry and response function of the system, can account for the possible formation of a charge-density wave (CDW) which could lead, through the electron-phonon coupling, to the renormalization of a phonon frequency, the corresponding phonon mode becoming overdamped at $T = T_c$, and driving the lattice to a new structural phase. This mechanism of a structural phase transformation proceeding via a soft-phonon mode is well known in other materials. Cochran[39] showed that many ferroelectric and antiferroelectric transitions result from a lattice instability to certain normal vibrational modes. Recently, the phonon-dispersion curves[40] of the well-known organic quasi-one-dimensional system tetrathiafulvalene-tetracyanoquinodimethane (TTF-TCNQ) have been found to show the existence of a Kohn anomaly at $k = 2k_F$, becoming deeper as the temperature reaches the Peierls transition temperature; the same phenomenon was also observed previously using the x-ray diffuse scattering technique.[41] The "one-dimensional" system $K_2Pt(CN)_4Br_{0.3}\cdot 3.2D_2O$ (KCP) also displays a giant Kohn anomaly.[42] As another example, the structural martensitic transition observed in some of the high-temperature superconducting A-15 compounds is thought to proceed via a Peierls instability in the linear chains of transition-metal atoms.[43,44] This mechanism is also closely related to the formation of charge-density waves observed in transition-metal dichalcogenides.[45]

The remainder of this paper is organized as follows: Section II is devoted to the description of the band structure and density of states of the metallic phase of VO_2 performed using the discrete variational method[46] (DVM) in a linear-combination-of-atomic-orbitals Bloch basis set; comparisons are made with previous theoretical predictions of the electronic structure[10,12] as well as with optical, soft-x-ray spectroscopy, and photoemission experiments. It has been widely recognized that the generalized electronic susceptibility function $\chi(\vec{q})$ plays an important role in the onset of charge-density waves,[47,48] spin-density waves,[49] lattice instabilities,[50] and phonon anomalies,[51] since instabilities of the system usually manifest themselves by anomalous increase in $\chi(\vec{q})$ at special values of the wave vector $\vec{q}$. In Sec. III we study the Fermi-surface geometry and report and analyze the features of the generalized susceptibility function, calculated in the constant-matrix-elements approximation. Using these results, we propose a possible interpretation of an electronically driven phase transformation for VO_2.

II. ELECTRONIC BAND STRUCTURE OF METALLIC VO_2

The rutile structure belongs to the nonsymmorphic space group D_{4h}^{14}. A study of the irreducible representations of this group can be found in the work of Gay *et al.*[52] The metal atoms form a body-centered-tetragonal array, with two vanadium atoms per unit cell; each is surrounded by a distorted octahedron of oxygen atoms in D_{2h} point-group symmetry. These octahedra share an edge along the c plane, whereas the octahedra surrounding the vanadium atoms at the corner and at the center of the cell share a common corner. The tetragonal unit cell and atomic positions as determined by Westman[8] were used in this work and are drawn in Fig. 1. More recent x-ray determinations of McWhan *et al.*,[33] however, suggest a smaller V-O distance and a smaller distortion of the ligand octahedra.

As noted by Goodenough[10] and Hearn,[53] the c/a ratio of VO_2 extrapolated to absolute zero temperature ($c/a = 0.621$) is smaller than the c/a ratio of an ideal purely ionic rutile structure determined by Pauling (0.66) and suggests a stronger bonding mechanism of the V atoms along the c axis.

In view of the convergence problems encountered in previous calculations and to solve the energy band problem to greater accuracy, we used an alternative scheme, the DVM, which permits use of a general crystal potential. Full details concerning the method have been given at length elsewhere[46]; we recall here the essential features. In the one electron approximation, the Hamiltonian H can be written

$$H(\vec{r}) = -\nabla^2 + V(\vec{r}) \tag{1}$$

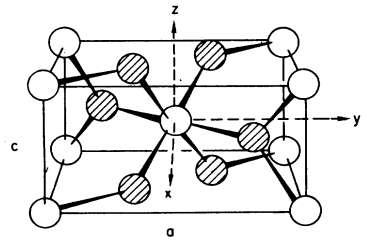

FIG. 1. Tetragonal unit cell of the rutile phase of metallic VO_2 (Ref. 8): $a = 8.579$ a.u., $c = 5.442$ a.u., $u = 0.305$. The atomic positions are: V $(0,0,0)$; V $(\frac{1}{2}a, \frac{1}{2}a, \frac{1}{2}a)$; O $(au, au, 0)$; O $(a(1-u), a(1-u), 0)$; O $(a(\frac{1}{2}-u), a(\frac{1}{2}+u), \frac{1}{2}c)$; O $(a(\frac{1}{2}+u), a(\frac{1}{2}-u), \frac{1}{2}c)$. Light spheres are vanadium atoms, striped spheres oxygen atoms; note sixfold coordination of vanadium to oxygen.

(we use Rydberg atomic units for energies and Bohr radii for length). In the case of VO_2, it is important to treat the full nonspherical crystal potential $V(\vec{r})$ accurately: there are six atoms in the unit cell; if one surrounds the nuclei with nonoverlapping spheres in the usual "muffin-tin" scheme, one cannot include more than $\frac{1}{3}$ of the total volume of the unit cell within the spheres. This clearly means that in this case, where substantial covalent bonding is expected, the commonly used approximation of a constant potential outside the spheres, as in the original APW or Korringa-Kohn-Rostoker (KKR) methods can lead to substantial inaccuracies. If these methods are to be used, it is essential to take into account the large variations of the crystal potential outside the muffin-tin spheres and to include a large number of basis functions in the interstitial region.

In the present work, the crystal potential is treated without spherical averaging procedures. The crystal charge density was approximated by a superposition of self-consistent atomic charge densities at a site ν, obtained from an atomic numerical program, using the $4s^2 3d^3$ configuration for V and $2s^2 2p^4$ for oxygen:

$$\rho(\vec{r}) = \sum_{\nu} \rho_{\nu}(\vec{r} - \vec{R}_{\nu}) \ . \tag{2}$$

The exchange potential is then calculated in the usual Slater local-exchange approximation as

$$V_{ex}(\vec{r}) = -6\alpha[(3/8\pi)\rho(\vec{r})]^{1/3} \ . \tag{3}$$

We used the full Slater exchange parameter value $\alpha = 1$, for the band structure as well as for the atomic calculations.

The crystal potential was then written as the sum of atomic Coulomb potentials and the exchange term

$$V(\vec{r}) = \sum_{\nu} V_{\text{Coul}}(\vec{r} - \vec{R}_{\nu}) + V_{ex}(\vec{r}) \ . \tag{4}$$

The wave function ψ_i for band state i and wave vector $\vec{k}$ was expanded as a linear combination of Bloch orbitals χ_j which are in turn constructed from a LCAO

$$\psi_i(\vec{k}, \vec{r}) = \sum_j \chi_j(\vec{k}, \vec{r}) C_{ji}(\vec{k}) \ , \tag{5}$$

$$\chi_j(\vec{k}, \vec{r}) = N^{-1/2} \sum_{\nu} e^{i\vec{k}\cdot\vec{R}_{\nu}} a_j(\vec{r} - \vec{R}_{\nu}) \ ; \tag{6}$$

the functions a_j are Slater-type orbitals (STO) centered at the corresponding sites ν. The basis set whose exponents are given in Table I included a total of 106 basis functions in the unit cell of which 35 STO's were used for each vanadium site and nine for each oxygen site.

By defining an error functional for state i as

$$\theta_i(\vec{r}) = (H - \epsilon_i)\psi_i(\vec{r}) \tag{7}$$

TABLE I. Slater-type orbitals used as basis set for this calculation, of the form $a(\vec{r}) = x^l y^m z^n r^p \exp(-\zeta r)$ at each atomic site.

V site					O site				
l	m	n	p	ζ	l	m	n	p	ζ
0	0	0	0	22.78	0	0	0	0	7.38
0	0	0	1	19.54	0	0	0	1	9.569
0	0	0	1	9.37	0	0	0	1	2.30
1	0	0	0		1	0	0	0	
0	1	0	0	19.54	0	1	0	0	3.692
0	0	1	0		0	0	1	0	
1	0	0	0		1	0	0	0	
0	1	0	0	9.37	0	1	0	0	1.656
0	0	1	0		0	0	1	0	
0	0	0	3	1.7					
0	0	0	3	1.4					
1	0	0	1						
0	1	0	1	5.4					
0	0	1	1						
1	0	0	1						
0	1	0	1	3.0					
0	0	1	1						
1	0	0	2						
0	1	0	2	1.7					
0	0	1	2						
1	0	0	3						
0	1	0	3	1.4					
0	0	1	3						
2	0	0	0						
0	2	0	0						
0	0	2	0	5.4					
1	1	0	0						
1	0	1	0						
0	1	1	0						
2	0	0	0						
0	2	0	0						
0	0	2	0	2.0					
1	1	0	0						
1	0	1	0						
0	1	1	0						

and minimizing the expectation values $\langle \chi_j / \theta_i \rangle$ over the grid of sampling points, one obtains the well-known matrix secular equation

$$(\underline{H} - \epsilon \underline{S})\underline{C} = 0 \ . \tag{8}$$

A reasonable compromise had to be made between the accuracy of the calculation and the growing size of matrices (Hamiltonian and overlap) evaluated with such a basis. The choice of the exponents of the STO's was guided by experience obtained from a previous molecular cluster model of vanadium oxides.[54] The matrix elements of the Hamiltonian were calculated numerically using a weighted sampling procedure, which avoids the well known difficulties found in evaluating multicenter integrals with an STO basis. In the present calculation, the matrix elements were evaluated at 6500 points in the unit cell; the param-

TABLE II. Parameters of the point distribution used in the numerical discrete evaluation of matrix elements of the Hamiltonian and overlap. N_0 is the number of sampling points inside a sphere of radius R_0 (in a.u.) surrounding each nucleus. N is the number of points taken in the interstitial region.

	R_0	N_0	N
Vsites	2.1	1300	...
O sites	1.5	500	...
Interstitial	...	...	1900

eters of the sampling point distribution are summarized in Table II. The pseudo random set of sampling points was not chosen with symmetry properties adapted to the crystal point group, so differences in the eigenvalues obtained for levels which should be degenerate by symmetry, gave evidence for the degree of convergence of the method; 6500 sampling points were necessary to obtain a convergence which is always better than 8 mRy even in the highest conduction bands.

The LCAO-DVM band calculation was performed at 30 inequivalent $\vec{k}$ points in the 1/16th irreducible wedge of the Brillouin zone (BZ) represented in Fig. 2; the a and b axis are divided into two parts, and the c axis into four parts. The energy eigenvalues were then fitted by a linear combination of 21 symmetrized plane waves leading to a maximum root-mean-square error of 3 mRy for the fitted points in the valence and conduction bands. The core level eigenvalues are also explicitly obtained in the LCAO method, but for convenience only the valence- and conduction-band states, in Rydberg units, are plotted along several high-symmetry

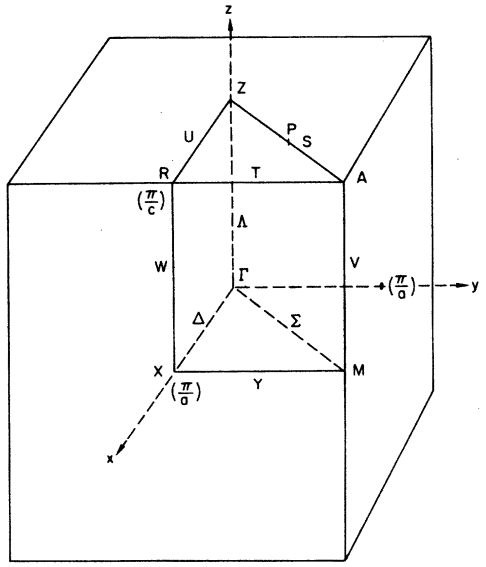

FIG. 2. The $\frac{1}{16}$ irreducible Brillouin zone of rutile phase of VO_2.

directions in Fig. 3. As the unit cell contains two molecules, there are 12 valence states and 10 conduction states; the lowest 12 bands in Fig. 3 form the oxygen $2p$ band, which has a maximum width $\simeq$4.6 eV at Γ.

An analysis of the wave functions at high-symmetry points shows that strong d components contribute to the lowest portion of the "O $2p$" valence band, due to the formation of covalent σ and π states between vanadium d and O $2p$ functions. At the top of the valence band, however, the V d component is negligible; these states are essen-

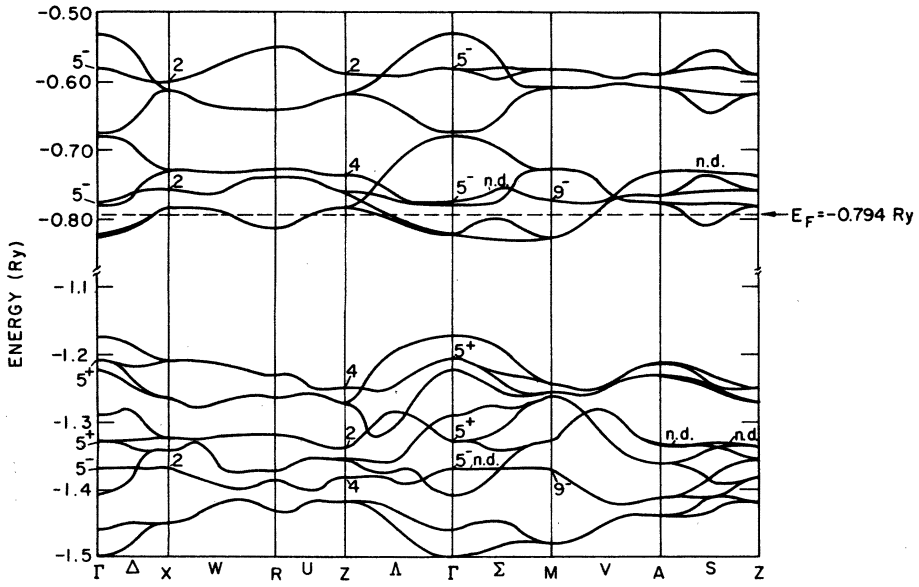

FIG. 3. "O $2p$" valence bands and "V $3d$" conduction bands of metallic VO_2 along several high-symmetry directions. Energies are in Ry. The near degeneracies (n.d.) of some bands are indicated.

tially O $2p$ in character. This observation is in agreement with the wave function analysis performed for a molecular cluster model of VO_2,[54] and also with the band results of Caruthers *et al.*[12] Since the twelve "O $2p$" states lie lower in energy than the metal d states, they will be fully occupied, leaving one electron per vanadium atom in the d bands.

A direct gap of ~4.6 eV at Γ separates the oxygen $2p$ valence band from the conduction states. The orthorhombic component of the crystal field splits the d states at Γ: the lowest six bands correspond to the "t_{2g}" symmetry states (for which the metal d functions point into regions between the ligands) split by the crystal field. The upper four bands arise from "e_g" states and are formed primarily by metal d orbitals pointing towards the ligands. However, an inspection of the linear variational coefficients of the wave functions shows that all the "e_g" states have strong O $2p$ components corresponding to antibonding V $3d$–O $2p$ states. The O $2p$ hybridization of the d "conduction states" is far smaller in the "t_{2g}" bands and negligible for the lowest-lying part of the t_{2g} manifold; these states result from V-V bonding along the c axis, in agreement with the phenomenological model of Goodenough.[10] This is also consistent with the experiment of Ladd and Paul[2] who found that, in the semiconducting regime just below T_c, the resistance decrease of VO_2 with stress along the c axis is far larger than with effect of stress on the basal plane (the reverse situation is found in V_2O_3); this suggested that in VO_2 the semiconducting gap opens up from states involving V-V interactions along the c axis; we find those states to be lying at the bottom of the d band in metallic VO_2. We found however other d-bonding components in the states below the Fermi energy; this is in agreement with the fact that the conductivity does not show a significant anisotropy.[55] The conduction band has a total width of 4 eV at Γ, the states arising from the splitting of the "t_{2g}" and "e_g" levels each having a 2-eV width. As can be seen in Fig. 3, the d bands (except for the lowest band in the Γ to M direction) show a non-negligible dispersion (of order 0.7 eV for the first band) and a certain amount of overlap and crossing. The Fermi energy falls at ~0.44 eV above the bottom of the d-band complex with "t_{2g}" character; the overlap of the partially filled lowest two conduction bands with higher bands accounts for the metallic conductivity. The low density of free carriers measured by Barker *et al.*[56] to be 2×10^{21} cm^{-3} is consistent with the quite small overlap found in the present calculation.

We calculated the density of states (DOS) from the Fourier series fit to the bands using an accurate integration scheme[57] in which we divided the $\frac{1}{16}$th of the irreducible zone into 1500 tetrahedra, and assumed the energy eigenvalues to vary linearly inside each microtetrahedron. The DOS of the valence- and conduction-band states, calculated on a 1-mRy mesh is plotted in Fig. 4. The Fermi energy is found to fall in a sharply rising portion of the DOS, at $E_F=-0.794$ Ry; there are ~144.4 (states of both spin)/(Ry unit cell) or ~10.63 (states of both spin)/(eV unit cell). This represents a large increase from the value of the DOS in vanadium metal [estimated to be ~2 states/(eV atom) (Ref. 58)].

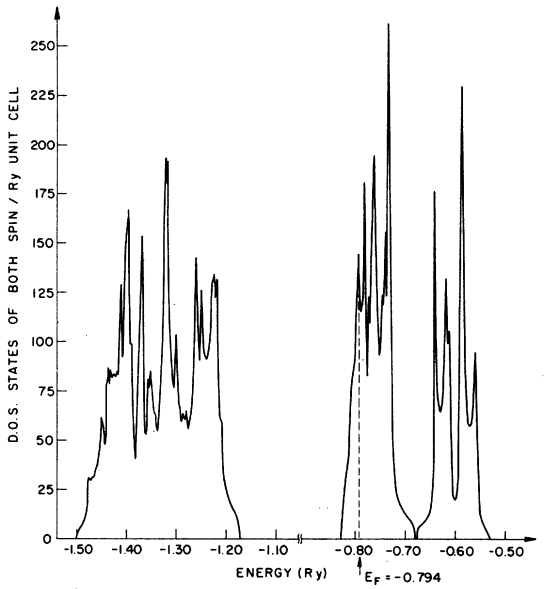

FIG. 4. Density of states for valence and conduction bands of metallic VO_2.

From $E=-0.830$ Ry at the bottom of the d bands, the DOS increases very sharply due to the flat portions of the bands at that energy, around Γ, and along Γ to M; another large contribution is expected near $E=-0.810$ Ry from flat parts of the degenerate bands around R and the bottom of the first conduction band in the AZ direction. The peak in the DOS at $E=-0.780$ Ry can be assigned to flat portions of the first two bands near X in the XR direction and near Z in the ZR and $Z\Gamma$ directions, from a flat portion of band 3 around Γ, and also from a flat segment of band 2 along the AZ direction. (The "d" bands are labeled here 1, 2, 3,... by increasing value of the energy.) Another peak in the DOS appears around $E=-0.764$ Ry due to flat portions of band 3 along AZ and around X in the $X\Gamma$ and XR directions. The largest peak in the $3d$ conduction band DOS occurs at $E=-0.734$ Ry and can be assigned to flat portions of bands 5 and 6 along X to R; A to Z, around R (in the R to Z direction), and around M (in the M to

A and M to Γ directions). This large peak is followed by an abrupt drop in the DOS, as in the energy range −0.734 to −0.680 Ry, only some portions of a single band (band 6) contribute. A very small gap of 0.004 Ry separates the e_g from the t_{2g} manifold. In the e_g band complex, the peak in the DOS at $E = -0.642$ Ry can be associated with flat portions of bands 7 and 8 around R in the RX and RZ directions and also in the AZ direction. The main peak in e_g manifold around $E = -0.585$ Ry comes essentially from flat portions of bands 8 and 9 along ΓZ, around M along MA and from band 9 along AZ.

The band calculation of Caruthers *et al.*[12] was performed, using a semiempirical warped muffin-tin potential; the energy eigenvalues were obtained with the APW method only at three high-symmetry points in the Brillouin zone, as up to 400 plane waves were required to obtain convergence. A Slater-Koster[59] fitting procedure was then used to obtain the entire band structure, the resulting rms error between APW and tight-binding eigenvalues being as large as 20 mRy. The general features of the DOS shown in Fig. 4 agree with the Caruthers *et al.*[12] results. We find more structure, because of our use of the accurate tetrahedron scheme,[57] compared to their rather coarse (~10-mRy) histogram mesh. Their larger overlap of the "t_{2g}" and "e_g" manifolds may be, in part, an artifact of the histogram method; it certainly is also due to the fact that the crystal potential used by these authors corresponds to a smaller V $3d$, O $2p$ interaction which causes a smaller splitting of the bonding and antibonding states. Their oxygen valence band is also raised in energy (leading to a smaller valence-conduction band gap) and the e_g states are lowered and show a greater overlap with t_{2g} states.

Finally, we emphasize that since the Fermi level falls in a region of large and strongly varying DOS, its position must be determined with care. For example, a shift of E_F by 2 mRy corresponds to a variation of 0.3 in the number of electrons.

Several experiments providing information about the valence and conduction bands of metallic VO_2 are available. Verleur *et al.*[17] studied the optical reflectivity and transmission spectra of metallic (and semiconducting) VO_2 between 0.25 and 5 eV and deduced, using a classical oscillator fit, the optical constants; the small peaks around ~2.8 and 3.6 eV in the imaginary part of the dielectric constant (also observed with small shifts in the low-T phase) were ascribed by them to interband transitions between the valence O $2p$ band and the unoccupied part of the conduction band. The structure observed around 2.8 eV, which is far broader and 1 eV lower in energy than the corresponding structure in TiO_2,[60] was found to be consistent with a band model in which a gap of ~2.5 eV separates the filled O $2p$ band from $3d$ conduction bands. Also, from the data of the semiconducting phase, the gap appearing in the $3d$ band was estimated to be ~0.6 eV. From their x-ray-photoelectron-spectroscopy (XPS) results, which show both a narrowing and a shift of the $3d$ DOS away from the Fermi energy in the low-T phase, Wertheim *et al.*[18] estimated the semiconducting gap to be ~0.7 eV. From an ultraviolet photoemission study, Powell *et al.*[61] estimated the position of the top of the valence band to be ~2.6 eV below the Fermi energy; in this data, however, the Fermi edge could not be resolved. More detailed information concerning the density of states of VO_2 has been obtained from XPS data, independently by Blaauw *et al.*[19] and Wertheim *et al.*[18] Their XPS spectrum is plotted in Fig. 5 along with our calculated DOS. We note that *direct* comparison of experiment with the total DOS cannot be performed due to the large ratio of V $3d$ to O $2p$ photoemission cross sections.[62] A detailed comparison of the experimental data with the band-structure results requires the knowledge of the oscillator strength matrix elements involved in the transition. Calculation of the required matrix elements was beyond the scope of the present investigations; thus, we will compare only the essential structure of the spectra with the information provided by the total density of states. The two sets of XPS data are in general agreement concerning the width of the occupied $3d$ band and the onset of the O $2p$ valence band. There are, however, some differences; the data of Blaauw *et al.*[19] shows a wider O $2p$ band and a different intensity structure. As noted by Wertheim *et al.*,[18] the XPS data show a wider occupied V $3d$ band than found in the band structure calculations (this either in ours or in that of Caruther *et al.*[12]); they attribute the structure of 1.3 eV to surface states, the XPS experiments being performed on thin films. The overall width of the O $2p$ band found in our calculation (4 eV) is in agreement with the XPS data; however, as in the case of the optical data[17] discussed above, this result cannot be compared to that of Caruther *et al.* since these authors chose a semiempirical potential which brings the calculated band gap into agreement with optical data.[17] The preliminary results of Chatterjee *et al.*[14] (using an *ab initio* crystal potential obtained by superposition of neutral atom charge densities) also led to a valence to conduction band gap considerably larger than experiment. The same conclusion was drawn from a molecular cluster model of VO_2.[54]

The x-ray vanadium $L_{II,III}$ emission and absorption spectra and the oxygen K emission band of

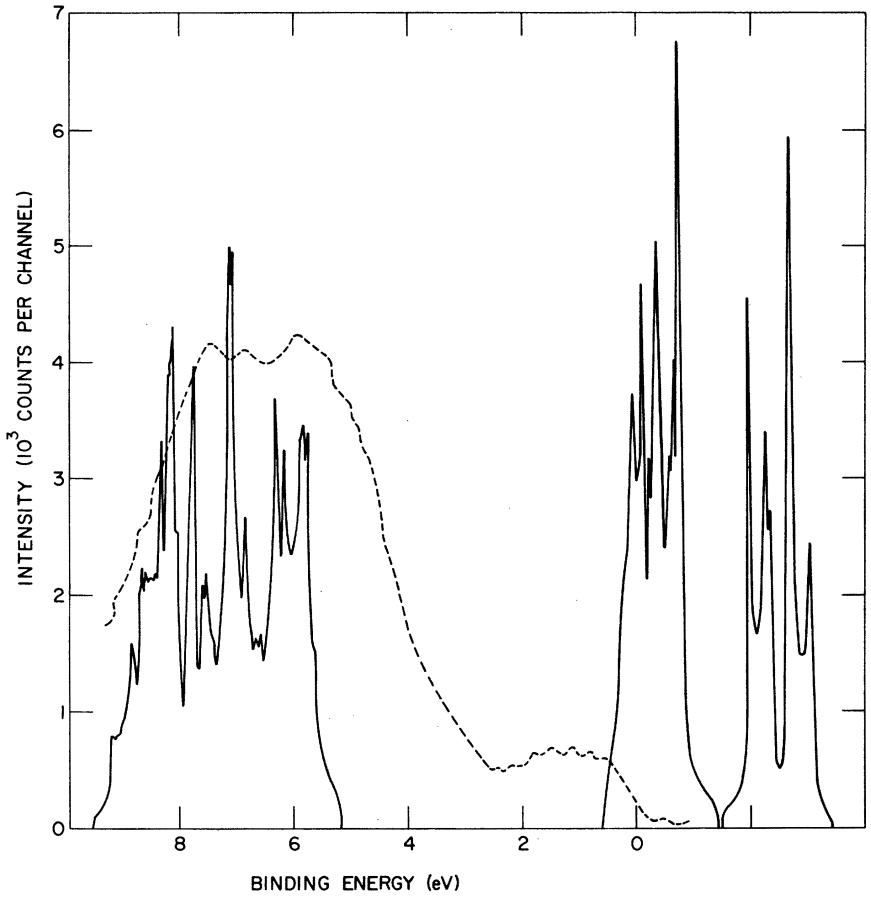

FIG. 5. Comparison of XPS data (Ref. 18, dashed curve) with density of states obtained in the present calculation (full line).

VO_2 are available,[63] but show no noticeable difference between the high- and low-temperature phases. According to the dipole selection rules, the L_{III} and L_{II} emission bands correspond, respectively, to $3d, 4s \rightarrow 2p_{3/2}$ and $3d, 4s \rightarrow 2p_{1/2}$ transitions. Figure 6 compares the vanadium $L_{II,III}$ emission spectrum found by Fischer[63] together with our total DOS. In Fischer's work, band A was attributed to O $2p \rightarrow$ V L_{III} crossover transitions; band B to V $3d \rightarrow$ V L_{III} normal emission, while structure D was expected to correspond to O $2s \rightarrow$ V L_{III} transition, and structure C

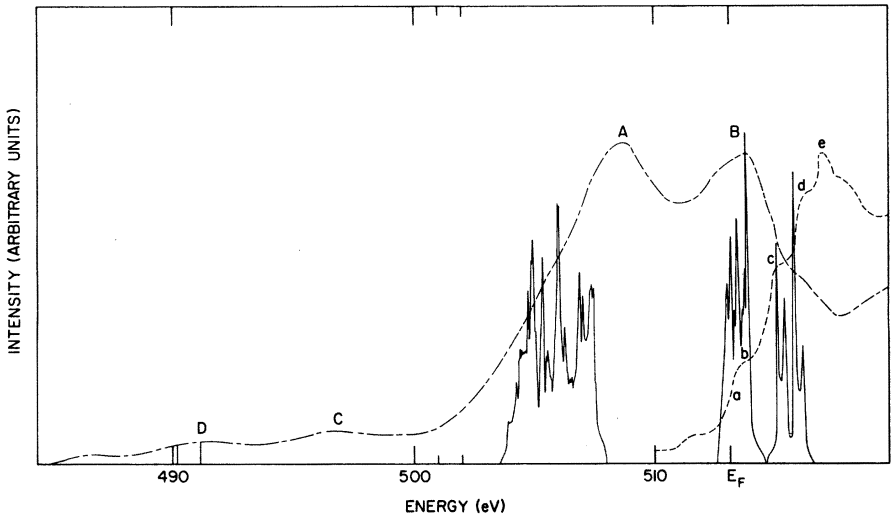

FIG. 6. Comparison of vanadium $L_{II,III}$ x-ray emission (broken line) and absorption (dashed line) spectra with theoretical DOS (full line).

to a combination of O $2s \rightarrow$ V L_{II} and V $M_{II,III} \rightarrow$ O $1s$. Band B can be compared to the total DOS of occupied conduction states because, as noted before, these states have a very small admixture of O $2p$ functions. Band A corresponds to the pure O $2p$ character of the valence band. We have already noted that pure O $2p$ character is found at the top of the band, while states at the bottom of the band have large V $3d$ covalent contributions. Thus the bottom of the band is expected to appear with a smaller intensity in the V $L_{II,III}$ spectrum. This qualitative observation agrees with the general shape of band A which shows a tail of low intensity on the low-energy side. The distance between peaks A and B, estimated by Fischer[63] to be 4.3 eV confirms the earlier observation that the gap between valence and conduction states in our calculation is too large. Note that the information given by band A of the V $L_{II,III}$ emission spectrum and by the XPS data are complementary, as the XPS spectrum is sensitive essentially to the d component of the band. The DOS of the O $2s$ band was not calculated but the vertical lines drawn in Fig. 6 indicate the position of this band from our calculation. It is found that the position of the O $2s$ band is in good agreement with the structure noted D in the spectrum.

The V $L_{II,III}$ absorption spectrum shows considerable structure.[63] The different humps denoted b, c, d, e, lie, respectively, 0.5, 2.1, 3.2, and 3.8 eV above the absorption edge denoted as a. These structures have to be associated essentially with the V $3d$ character of the bands, as the V $4s$ contribution in this energy range is negligible. Our calculation of the width of the unoccupied conduction states with d character agrees with that obtained from the x-ray absorption spectrum. The total density of unoccupied conduction states in our calculation shows even more fine structure than observed. However, it is meaningless to assign a one-to-one correspondence between experimental and theoretical features without a projection of the DOS onto its angular momentum components and a calculation of the oscillator-strength matrix elements.

The observed oxygen K emission band[63] corresponding to O $2p \rightarrow$ O $1s$ transitions is reproduced in Fig. 7. Structure C was found to be strongly dependent on the dispersing crystal and will not be discussed here. The main peak labeled B arises from the oxygen $2p$ valence-band states. The width of this band is in good agreement with the result of the present calculation. Perhaps the little shoulder between peak B and structure C is due to the subsidiary O $2p$ character of the occupied V $3d$ states; it is, however, extremely small, as indicated by our calculation.

The general features of the band-structure calculation are thus in reasonable agreement with experimental spectra, with the notable exception of the O $2p$–V $3d$ gap. A self-consistent potential, in giving a better account of the charge transfer from the vanadium to the oxygen ions could reduce the magnitude of the O $2p$–V $3d$ gap and give better agreement with the x-ray, XPS, and optical data; however, the method presently used will have to be improved with respect to computing time before such calculations are feasible. We should also point out that a theoretical determination of the O $2p$–V $3d$ band gap for direct comparison with previously quoted experiments requires the evaluation of energy differences between excited and ground states of the system; in this paper, we are only concerned with ground-state properties.

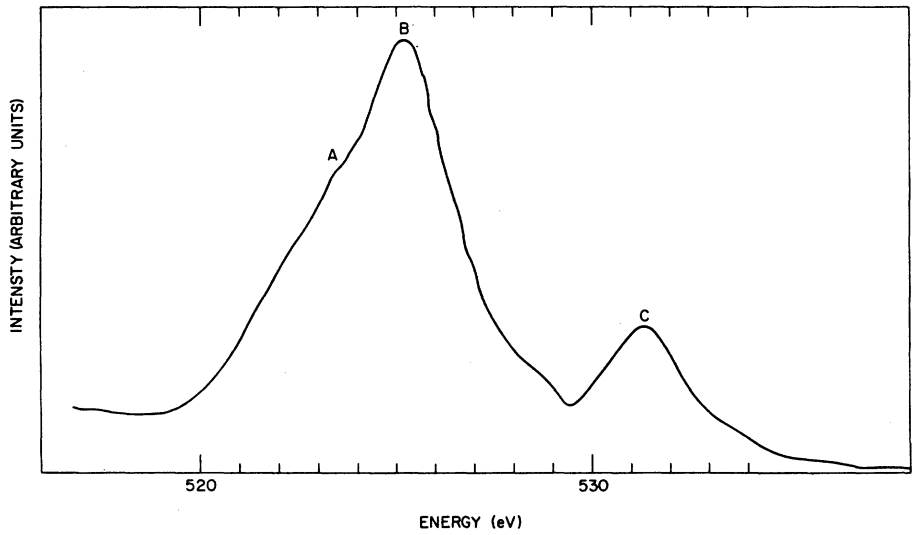

FIG. 7. Oxygen K emission spectrum of Ref. 63.

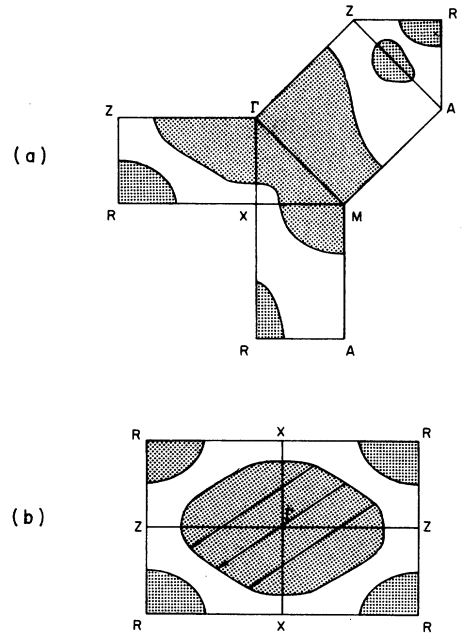

FIG. 8. (a) Fermi-surface cross sections of the lowest "V 3d" conduction band (band 1) on high-symmetry planes determining boundaries of the $\frac{1}{16}$th irreducible Brillouin zone. Shaded portions indicate the occupied regions. (b) Fermi-surface cross section of band 1 in the ΓZR plane. Shaded portions indicate occupied regions; arrows indicate the nesting vector $\vec{q} \simeq \Gamma R$.

III. FERMI-SURFACE GEOMETRY AND GENERALIZED SUSCEPTIBILITY FUNCTION

A. Fermi surface

As stated previously we find that the Fermi surface (FS) of VO_2 is determined by the first two lowest d bands. Each band is partially filled leading to electron surfaces around Γ, M, and R. For band 1, which contains 66.4% of the two electrons occupying the conduction bands, there is a supplementary electron surface centered around the middle of ZA. The FS cross sections in the high-symmetry planes forming the boundary of the $\frac{1}{16}$th irreducible wedge of the BZ are given in Figs. 8 and 9, for bands, 1 and 2 respectively.

The most noticeable features for the band 1 FS cross section is the existence of flat portions (cf. ΓXRZ plane) which nest into each other when translated by $\vec{q} = (\frac{1}{2}, 0, \frac{1}{2})$. Similar cross sections are found in the planes perpendicular to the y axis with origins $(0,0,0) \leq \vec{q} \leq (0.2, 0.2, 0.2)$, leading to a "cylinder" of small height along the y axis. The "nesting" observed in this Fermi surface is however limited, due to the small height of the cylinder. We shall see further how this feature affects the response function of the conduction electrons of this system.

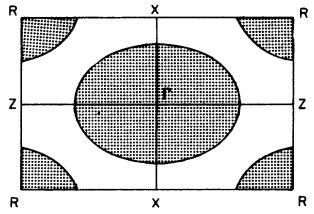

FIG. 9. Fermi-surface cross section of band 2 in the ΓZR plane; shaded portions indicate occupied regions.

Although Caruthers *et al.*[12] did not give the Fermi-surface cross sections resulting from their calculation, inspection of their bands plotted in several symmetry directions indicates some similarities and differences with the present results. In addition to bands 1 and 2 crossing E_F, their results have very small electron pockets around Γ due to bands 3, 4, 5. However, as observed in the present work, the major contribution to the Fermi surface arises from bands 1 and 2. The difference concerning bands 1 and 2 is the size of the electron pocket around R (larger in the Caruthers *et al.* calculation) compensated by a smaller size of the electron surface around Γ. Also, in the work of Caruthers *et al.*,[12] the electron surfaces for bands 1 and 2 around Γ are not connected to the piece around M, contrary to our result. However, the major features of the FS, essentially determined by the first two bands forming electron pockets around Γ, M, R, and for the first band around the middle of ZA, is common to the two calculations. We attribute the differences between the two calculations concerning bands 1 and 2 Fermi surfaces, in large part to the interpolation procedure used by Caruthers *et al.*[12] based only on three calculated *ab initio* points in the Brillouin zone. This restriction was of course dictated by the difficulty of the calculation. We do not think that differences in the crystal potential would strongly affect the shape of the Fermi surface for the following reason: since, in the lower part of the "t_{2g}" manifold (where the states have essentially a V 3d character and the residual O 2p admixture of the wave functions is negligible, the shape of the bands which determine the FS will not be very sensitive to differences in the overlap or charge transfer from the vanadium to the oxygen atom. It is very unlikely that self-consistent iterations would change the main features of the Fermi surface found in the present calculation.

B. Generalized susceptibility

The band structure of the conduction states was used to evaluate the generalized susceptibility function of the system. In the random-phase approximation, the wave vector and frequency-de-

pendent dielectric function can be written

$$\epsilon(\vec{q},\omega) = 1 + (4\pi e^2/\Omega q^2)\chi(\vec{q},\omega) \ , \tag{9}$$

$$\chi(\vec{q},\omega) = \chi_1(\vec{q},\omega) + i\,\chi_2(\vec{q},\omega)$$

$$= -\sum_{kk'} \frac{f_k - f_{k'}}{E_k - E_{k'} + \hbar\omega + i\delta} \times \langle\psi_k|e^{-i\vec{q}\cdot\vec{r}}|\psi_{k'}\rangle\langle\psi_{k'}|e^{i\vec{q}\cdot\vec{r}}|\psi_k\rangle \ , \tag{10}$$

where E_k, ψ_k, f_k are, respectively, the energy eigenvalue, wave function, and occupation number of state k (k stands for both wave vector $\vec{k}$ and band index n). $\sum_{kk'}$ refers to the integration over the Brillouin zone. The oscillator strength matrix element in Eq. (10) imposes the restriction $\vec{k}' = \vec{k} + \vec{q} + \vec{G}$, where $\vec{G}$ is a reciprocal-lattice vector.

The importance of the imaginary part of $\epsilon(\vec{q},\omega)$ for reflectivity, and dynamical form factors is very well known. The static susceptibility function

$$\mathrm{Re}\chi(\vec{q},\omega=0) = -\sum_{kk'} \frac{f_k - f_{k'}}{E_k - E_{k'}} |M_{\vec{k}\vec{k}'}(\vec{q})|^2 \tag{11}$$

also contains interesting physical information, as it measures to first order the response of the electrons to a perturbation; its important role in the onset of electronic instabilities such as spin-density waves[49] (SDW), CDW,[48] and also lattice instabilities,[50] is expected.

In the case of CDW (or SDW), a lower energy resulting from the promotion of electrons from orbitals with one spin to orbitals of the same (or opposite) spin, can be sustained by the Fermi-surface geometry since a nesting feature is favorable to the promotion of electrons from an electron to a hole portion of the Fermi surface. This repopulation can be also achieved by the scattering of the electrons by phonons through the electron phonon interaction. It can be shown that the generalized susceptibility function $\chi(\vec{q})$ plays an important role in the expression of the renormalized phonon frequencies and that, under simplifying assumptions, a divergence in $\chi(\vec{q})$ can lead to a softening of the corresponding vibrational mode. Recently, we interpreted[64] anomalies in the phonon dispersion curves of high-temperature superconducting transition-metal carbides in terms of an overscreening of the corresponding lattice vibration by the conduction electrons which manifests itself by large values of $\chi(\vec{q})$ at certain $\vec{q}$ values. The correlation between Fermi-surface features and anomalies in the phonon-dispersion curves was first proposed by Kohn[51] for a free-electron gas. Note that in this case, while $\chi(\vec{q})$ does not show any divergence at $2k_F$, a divergence in its gradient can cause a discontinuity in the gradient of $\omega_{\vec{q}}$ and thus lead to a "kink" (Kohn anomaly) in the phonon spectrum. We should recall that besides the importance of $\chi(\vec{q})$ in the formation of a SDW CDW state or in phonon anomalies, other factors such as the electronic Coulomb, exchange and correlation interactions, as well as the electron-phonon matrix elements play a major role. The interplay of these different quantities in producing a SDW versus a CDW ground state coupled to a periodic lattice distortion has been discussed by Chan and Heine.[48]

We will focus here on the physical information contained in the generalized susceptibility function alone. As can be seen from Eq. (11) maxima in the susceptibility can occur when states of different occupancy are connected by a wave vector $\vec{q}$. This is the case when large portions of the Fermi surface "nest" into each other by translation with vector $\vec{q}$ or if flat parallel bands can be connected by a given vector $\vec{q}$ ("volume effect").

The calculation of matrix elements (ME), when performed with actual Bloch functions and accurate integration procedures is not a trivial task[65]; approximate methods using tight-binding functions have been also used.[66] Even though an accurate calculation of the matrix elements would be desirable, we believe, however, that the susceptibility in the constant ME approximation contains essential physical information through the energy-dependent term. In the present calculation, we assumed the oscillator-strength matrix elements to be constant and we discuss separately intraband and interband contributions to the susceptibility, since it is well known that the matrix elements affect them in very different ways. Using the Wannier representation of the Bloch functions[67] it can be shown that the matrix elements multiply the intraband contribution by a function behaving like the square of an atomic form factor, i.e., slowly decreasing away from the zone center. By contrast, the (usually large) value of the interband transitions becomes identically zero at $\vec{q}=0$ when matrix elements are included and, if the interband part does not show any prominent feature, the effect of matrix elements will be largely to suppress the background arising from the interband contribution.

The Brillouin-zone integration required in Eq. (11) was performed by means of an accurate analytic linear-energy tetrahedron scheme,[68] similar to that used for the density-of-states calculation. With 1500 tetrahedra in the $\frac{1}{16}$th irreducible wedge of the BZ, we recovered from the intraband contribution in the $q \to 0$ limit the value of the density of states at E_F with an accuracy better than 1%.

The intraband contributions from bands 1 and 2 and the total interband contributions from the six bands belonging to the t_{2g} manifold are plotted separately in Fig. 10, along three high-symmetry directions ΓR $(1,0,1)$; ΓP $(\frac{1}{2},\frac{1}{2},1)$ and RP $(\xi,\frac{1}{2}-\xi,\frac{1}{2})$. The total intraband value increases away

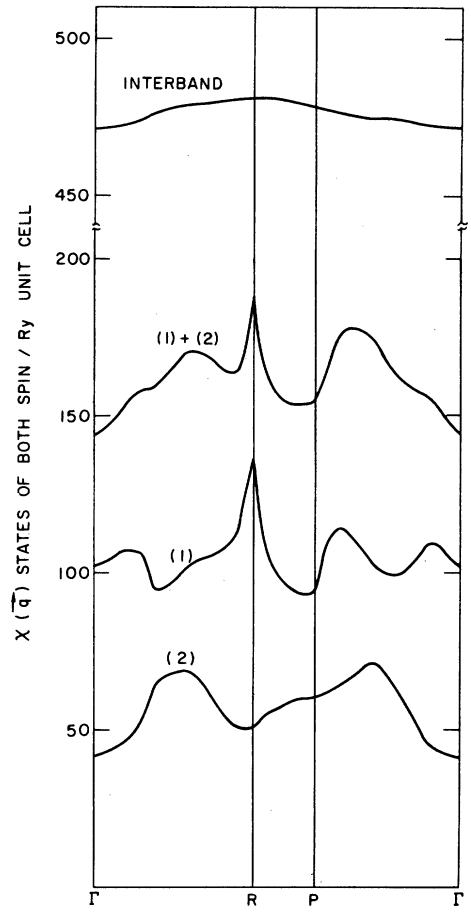

FIG. 10. The generalized susceptibility function $\chi(\vec{q})$ of metallic VO_2 is given along several symmetry directions, with contributions from the lowest six "V $3d$" conduction bands. Curve (1) is the intraband contribution of band 1; curve (2) the intraband contribution of band (2); the curve labeled (1) + (2) is the total intraband contribution. The upper curve is the sum of all *interband* contributions from the six bands belonging to the fully split "t_{2g}" manifold; note the break in the vertical scale.

from Γ and shows a sharp rise at the zone boundary R. The peak at R in the intraband function corresponds to a 29% increase from the value at Γ; this peak is due to the band-1 contribution and can be associated with the "nesting" features with wave vector $\vec{q} = (\frac{1}{2}, 0, \frac{1}{2})$ mentioned above. Due to the accuracy of the band calculation, we checked that a shift in the Fermi energy by 2 mRy did not affect the peak obtained at R in the intraband contribution; we found that the overall magnitude of the $\chi(\vec{q})$ curve was reduced, as it scales with the value of the DOS at E_F, but the peak at R remained, becoming slightly broader. The magnitude of band-1 contribution to $\chi(\vec{q})$ is generally 50% higher than the band-2 contribution throughout the Brillouin zone. This latter contribution shows in the ΓR direction a broad structure for $0.3 < q < 0.8$ associated with contributions from the FS piece around Γ, as the electron pocket around R has essentially the same characteristics for both bands.

The total interband contribution is remarkably flat and the resulting large background which it provides to the total $\chi(\vec{q})$ would be largely suppressed by the effect of the matrix elements. As no noticeable structure can be observed in the interband part, this contribution will be ignored in the rest of the discussion.

The ΓP direction is also interesting for study as the second-order phase transition of the isoelectronic compound NbO_2 is thought to be driven by a soft phonon at the zone boundary P, and the existence of a CDW with wave vector $\vec{q} = \Gamma P$ has been proved after observation of critical scattering by elastic neutron diffraction.[35] As shown in Fig. 10, the total intraband contribution increases away from Γ in the ΓP direction. The band-2 contribution has the same features as in the ΓR direction but the band-1 contribution drops for $\vec{q} > (0.4, 0.4, 0.8)$ and does not show a peak at the zone boundary P. The total intraband susceptibility has a broad maximum around $\vec{q} = (0.45, 0.45, 0.9)$; the height of this structure is smaller, however, than the sharp peak at R found in the ΓR direction. Even though NbO_2 is isoelectronic to VO_2, details of the electronic structure of the two compounds are expected to be different. The larger binding of the Nb atoms in NbO_2 compared to the atoms in VO_2, in the monoclinic as well as in the rutile phase, is confirmed by the far larger transition temperature $T_c = 1081$ K for NbO_2 $T_c = 341$ K for VO_2. Also, the c/a ratio is smaller for NbO_2 than for VO_2 and TiO_2 indicating stronger metal-metal bonding along the c axis for Nb. The interaction of two Nb atoms along the c axis is certainly stronger than that for two V atoms in VO_2, as the $4d$ atomic functions have a larger spatial extension than the $3d$ functions and this stronger overlap cannot be compensated by the small increase in length of the c axis from VO_2 to NbO_2. Consequently, the width of the Nb $4d$ band is expected to be larger. This could lead to substantial differences in the details of the conduction bands and consequently to a different Fermi surface and a possible shift of the structure observed around $\vec{q} = (0.45, 0.45, 0.9)$ towards the zone boundary at the P point. This possibility cannot however be ruled out without a detailed study of the electronic structure of NbO_2. We also note that for this compound, a different explanation which does not invoke an anomalous behavior in $\chi(\vec{q})$ at the point P, has been proposed.[69]

Strong x-ray diffuse scattering has been ob-

served[36] along the *RP* direction in reciprocal space for the nonstoichiometric alloy $V_{0.9}Nb_{0.1}O_2$. Based on experiments in VO_2, NbO_2, and $V_xNb_{1-x}O_2$, the *RP* segment has been thought to be the locus of the soft phonon modes responsible for the structural phase transformation. We should recall however that for $V_{0.9}Nb_{0.1}O_2$, the metal-to-semiconductor transition is not accompanied by a full structural phase transformation but by a local bidimensional ordering with a pairing of V atoms in the (110) planes of the rutile structure, with little correlation between these planes.[36] Since, from Fig. 10, $\chi(\vec{q})$ drops constantly from R to P the conduction electrons of VO_2 do not show any anomalous behavior in this direction. However, $\chi(\vec{q})$ is highly sensitive to details of the electronic structure; its detailed behavior can be expected to be modified upon alloying from that obtained for VO_2.

The results for $\chi(\vec{q})$ determined for VO_2 along these several symmetry directions show an absolute maximum to occur at the point R in reciprocal space, which arises essentially from the FS nesting features of the lowest conduction band. Thus, the response function of the conduction electrons of the system shows an instability at the zone boundary R. The Fermi surface can sustain a charge density wave and, even though the phase transition for VO_2 is first order in nature, this instability could manifest itself by an overdamping of the corresponding phonon mode with wave vector $\vec{q} = (\frac{1}{2}, 0, \frac{1}{2})$, due to the renormalization of this mode through the electron phonon coupling. This particular vector is compatible with the change from rutile to monoclinic structure[37] and leads to a doubling of the unit cell in the low-temperature phase.

Our calculation of the response function shows that it may be possible to interpret the structural phase transformation in VO_2 in terms of a condensation of phonons at the point R of the rutile Brillouin zone. No definite conclusion can be drawn from the present calculation about the isoelectronic NbO_2 compound because the dielectric susceptibility is sensitive to the details of the band structure and quantitative changes are expected for NbO_2 in view of the stronger metal-metal interaction in this compound.

---

*On leave from la Faculté des Sciences, Orsay, France and le Centre de Mécanique Ondulatoire Appliquée, 23 rue du Maroc, 75019 Paris, France.

†Supported by the NSF (through the Northwestern Univ. MRC), AFOSR, and U. S. ERDA.

[1]F. J. Morin, Phys. Rev. Lett. 3, 34 (1959).
[2]L. A. Ladd and W. Paul, Solid State Commun. 7, 425 (1969).
[3]W. G. Rudorff, G. Walter, and J. Stadler, Z. Anorg. Allg. Chem. 297, 1 (1958).
[4]D. Alder, in *Solid State Physics* (Academic, New York, 1968), Vol. 21, p. 1.
[5]W. G. Rudorff, G. Walter, and J. Stadler, Z. Arnog. Allgem. Chem. 297, 1 (1958); T. Kawakubo and T. Nakagawa, J. Phys. Soc. Jpn. 19, 517 (1964).
[6]K. Kosuge, J. Phys. Soc. Jpn. 22, 251 (1967).
[7]J. Umeda, H. Kusumoto, K. Narita, and E. Yamada, J. Chem. Phys. 42, 1458 (1965).
[8]S. Westman, Acta. Chem. Scand. 15, 217 (1961).
[9]G. Anderson, Acta. Chem. Scand. 8, 1599 (1954); 10, 623 (1956).
[10]J. B. Goodenough, Bull. Soc. Chim. France 4, 1200 (1965); Phys. Rev. 117, 1442 (1966); in *Progress in Solid State Chemistry*, edited by H. Reiss (Pergamon, Oxford, 1971), Vol. 5, p. 145; J. Solid State Chem. 3, 490 (1971).
[11]J. P. Pouget, P. Lederer, D. S. Schreiber, H. Launois, D. Wohlleben, A. Casalot, and G. Villeneuve, J. Phys. Chem. Solids 33, 1961 (1972).
[12]E. Caruthers, L. Kleinman, and H. I. Zhang, Phys. Rev. B 7, 3753 (1973).
[13]T. K. Mitra, S. Chatterjee, and G. J. Hyland, Can. J. Phys. 51, 352 (1973).
[14]S. Chatterjee, T. K. Mitra, and G. J. Hyland, Phys. Lett. A 42, 56 (1972).
[15]L. F. Mattheiss, Phys. Rev. B 13, 2433 (1976).
[16]N. Daude, C. Gout, and C. Jouanin, Phys. Rev. B 15, 3229 (1977).
[17]H. W. Verleur, A. S. Barker, and C. N. Berglund, Phys. Rev. 172, 788 (1968).
[18]G. K. Wertheim, M. Campagna, H. J. Guggenheim, J. P. Remeika, and D. N. E. Buchanan, AIP Conf. Proc. 24, 235 (1974).
[19]C. Blaauw, F. Lennhouts, F. Van der Woude, and G. A. Sawatzky, J. Phys. C 8, 459 (1975).
[20]A. Zylbersztejn and N. F. Mott, Phys. Rev. B 11, 4383 (1975).
[21]W. F. Brinkman and T. M. Rice, Phys. Rev. B 2, 4302 (1970).
[22]E. Caruthers and L. Kleinman, Phys. Rev. B 7, 3760 (1973).
[23]D. Adler and H. Brooks, Phys. Rev. 155, 826 (1967).
[24]D. Adler, J. Feinleib, H. Brooks, and W. Paul, Phys. Rev. 155, 851 (1967).
[25]C. N. Berglund and H. J. Guggenheim, Phys. Rev. 185, 1022 (1969).
[26]W. Paul, Mat. Res. Bull. 5, 691 (1970).
[27]C. J. Hearn, Phys. Lett. A 38, 447 (1972).
[28]J. P. Pouget, H. Launois, T. M. Rice, P. Dernier, A. Gossard, G. Villeneuve, and P. Hagenmuller, Phys. Rev. B 10, 1801 (1974).
[29]P. Lederer, H. Launois, J. P. Pouget, A. Casalot, and G. Villeneuve, J. Phys. Chem. Solids 33, 1969 (1972).
[30]L. A. Ladd, Technical Report, Harvard University No. M.P. 26, ARPA-41 (1971) (unpublished).
[31]R. Srivastava and L. L. Chase, Phys. Rev. Lett. 27, 727 (1971).
[32]A. Mooradian and P. M. Raccah, Phys. Rev. B 3, 4253 (1971).
[33]D. B. McWhan, M. Marezio, J. P. Remeika, and P. D.

Dernier, Phys. Rev. B 10, 490 (1974).
[34]M. Marezio, D. B. McWhan, J. P. Remeika, and P. D. Dernier, Phys. Rev. B 5, 2541 (1972).
[35]S. M. Shapiro, J. D. Axe, G. Shirane, and P. M. Raccah, Solid State Commun. 15, 377 (1974); we note, however, that the soft-phonon picture for NbO_2 has recently been questioned by R. Pynn, J. D. Axe, and R. Thomas (unpublished).
[36]R. Comès, P. Félix, M. Lambert, and G. Villeneuve, Acta. Crystallogr. A 30, 55 (1974).
[37]J. R. Brews, Phys. Rev. B 1, 2557 (1970).
[38]J. Y. Prieur, P. Seznec, and S. Ziolkiewicz, J. Phys. Lett. 38, L25 (1977).
[39]W. Cochran, Adv. Phys. 9, 387 (1960).
[40]G. Shirane, S. M. Shapiro, R. Comès, A. F. Garito, and A. J. Heeger, Phys. Rev. B 14, 2325 (1976); H. A. Mook and C. R. Watson, Phys. Rev. Lett. 36, 801 (1976).
[41]F. Denoyer, R. Comès, A. F. Garito, and A. J. Heeger, Phys. Rev. Lett. 35, 445 (1975); S. Kagoshima, H. Anzai, K. Kajimura, and T. Ishigoro, J. Phys. Soc. Jpn. 39, 1143 (1975).
[42]K. Carneiro, G. Shirane, S. A. Werner, and S. Kaiser, Phys. Rev. B 13, 4258 (1976).
[43]L. P. Gorkov, JETP Lett. 17, 379 (1973); L. P. Gorkov and O. N. Dorokhov, J. Low Temp. Phys. 22, 1 (1976).
[44]G. Bilbro and W. L. McMillan, Phys. Rev. B 14, 1887 (1976).
[45]J. A. Wilson, F. J. DiSalvo, and S. Mahajan, Adv. Phys. 24, 117 (1975).
[46]D. E. Ellis and G. S. Painter, Phys. Rev. B 2, 2887 (1970).
[47]A. W. Overhauser, Phys. Rev. B 3, 3173 (1971).
[48]S. K. Chan and V. Heine, J. Phys. F 3, 795 (1973).
[49]A. W. Overhauser, Phys. Rev. 128, 1437 (1962); W. M. Lomer, Proc. Phys. Soc. Lond. 80, 489 (1962); C. Herring, in *Magnetism*, edited by G. T. Rado and H. Suhl (Academic, New York and London, 1966), Vol. 4.
[50]S. H. Liu, Phys. Rev. B 10, 3619 (1974).
[51]W. Kohn, Phys. Rev. Lett. 2, 393 (1959).
[52]J. G. Gay, W. A. Albers, Jr., and F. J. Arlinghaus, J. Phys. Chem. Solids 29, 1449 (1968).
[53]C. J. Hearn, Solid State Commun. 12, 53 (1973).
[54]Michèle Gupta and D. E. Ellis, Phys. Rev. B 13, 3405 (1976); V. A. Gubanov and D. E. Ellis, J. Struc. Chem. (USSR) 17, 962 (1976).
[55]P. F. Bongers, Solid State Commun. 3, 275 (1965).
[56]A. S. Barker, Jr., H. W. Verleur, and H. J. Guggenheim, Phys. Rev. Lett. 17, 1286 (1966).
[57]O. Jepsen and O. K. Anderson, Solid State Commun. 9, 1763 (1971); G. Lehman, P. Renert, M. Taut, and H. Wonn, Phys. Status Solidi 37, K27 (1970); G. Lehman and M. Taut, *ibid*. 54, 469 (1972).
[58]L. L. Boyer, D. A. Papaconstantopoulos, and B. M. Klein, Phys. Rev. B 15, 3685 (1977).
[59]J. C. Slater and G. F. Koster, Phys. Rev. 94, 1498 (1954).
[60]M. Cardona and G. Harbeke, Phys. Rev. 137, 1467 (1965).
[61]R. J. Powell, C. N. Berglund, and W. E. Spicer, Phys. Rev. 178, 1410 (1969).
[62]G. K. Wertheim, L. F. Mattheiss, M. Campagna, and T. P. Pearsall, Phys. Rev. Lett. 32, 997 (1974).
[63]D. W. Fischer, J. Appl. Phys. 40, 4151 (1969).
[64]Michèle Gupta and A. J. Freeman, Phys. Rev. Lett. 37, 364 (1976); Phys. Lett. A 57, 291 (1976); Phys. Rev. B 14, 5205 (1976).
[65]R. P. Gupta and S. K. Sinha, Phys. Rev. B 3, 2401 (1971); R. P. Gupta and A. J. Freeman, *ibid*. 13, 4376 (1976).
[66]J. F. Cooke, H. L. Davis, and Mark Mostoller, Phys. Rev. B 9, 2485 (1974).
[67]R. M. Pick, in *Phonons, Proceedings of the International Conference on Phonons, Rennes, 1971*, edited by M. A. Nusimovici (Flammarion, Paris, 1972), p. 20; W. Hanke and H. Bilz, in *Proceedings of the International Conference on Inelastic Scattering of Neutrons* (IAEA, Vienna, 1972), p. 3.
[68]J. Rath. R. P. Gupta, and A. J. Freeman, AIP Conf. Proc. 24, 327 (1975); J. Rath and A. J. Freeman, Phys. Rev. B 11, 2109 (1975).
[69]S. K. Das and S. K. Sinha, Bull. Am. Phys. Soc. 22, 474 (1977); and S. K. Sinha (private communication).